Electronic Supplementary Information for

Hydrogen-intercalation PdZn bimetallene for urea electro-synthesis from nitrate and carbon dioxide

Ziqiang Wang, Yanan Wang, Shan Xu, Kai Deng, Hongjie Yu, You Xu,

Hongjing Wang* and Liang Wang*

State Key Laboratory Breeding Base of Green-Chemical Synthesis Technology, College of Chemical Engineering, Zhejiang University of Technology, Hangzhou 310014, P. R. China

E-mails: hjw@zjut.edu.cn; wangliang@zjut.edu.cn

Characterizations

Scanning electron microscopy (SEM, ZEISS Gemini 500) and transmission electron microscopy (TEM, JEOL JEM-2100F) were used to characterize the microscopic morphology of the catalyst. The crystal structure of the catalysts was determined by X-ray diffraction (XRD, DX-2700). X-ray photoelectron spectroscopy (XPS, ULVAC PHI Quantera) was used to determine the chemical states of the elements in the catalysts. The thickness of the catalyst was measured using an atomic force microscope (AFM, NT-MDT Prima). Nuclear magnetic resonance (NMR) spectra were obtained using a superconducting magnet NMR spectrometer (Germany Bruker 600MHz).

Product determination

The urea was measured by the diacetyl monoxime method.[1] Firstly, 30 mL H_2SO_4 and 10 mL H_3PO_4 were added to 60 mL deionized water, and then 10 mg $FeCl_3$ was dissolved in the above solution (solution A). Then, 0.5 g of DAMO and 10 mg of TSC were dissolved in 100 mL deionized water (solution B). After that, 80 μL of electrolysis solution was taken from cell and diluted into 1 mL solution, mixing with 2 mL of solution A and 1 mL of solution B on heating at 110 ℃ for 15 min. The absorbance of mixed solution was measured at 525 nm using UV-vis spectrophotometer. The R_{urea} and FE_{urea} of urea synthesis were calculated by the following equations:

$$R_{urea} = C_{urea} \times V/(t \times m) \quad (1\text{-}1)$$

$$FE_{urea} = (16 \times F \times C_{urea} \times V)/(60.06 \times Q) \times 100\% \quad (1\text{-}2)$$

where C_{urea} and V are the measured concentration of urea and the total volume of the cathodic electrolyte, respectively; t is the reduction time and m is the metal of the loaded electrocatalyst; F is the Faraday constant (96,485 C mol^{-1}), Q (C) is the total electric quantity during each current

passage.

The concentration of product NH_3 was determined by indophenol blue method.[2] Firstly, the electrolyte is removed from the cell and diluted into 2 mL solution, followed by adding 2 mL of 1 M NaOH solution containing 5 wt% $C_7H_6O_3$ and 5 wt% $C_6H_5Na_3O_7$, 1 mL of 0.05 M NaClO solution and 0.2 mL of 1 wt% $C_5FeN_6Na_2O$ solution. After reaction for 2 h at room temperature, the absorbance of mixed solution was measured using UV-vis spectrophotometer at a wavelength of 655 nm. The R_{NH3} and FE_{NH3} of ammonia synthesis were calculated using the following equations:

$$R_{NH3} = C_{NH3} \times V/(t \times m) \quad (1\text{-}3)$$

$$FE_{NH3} = 8 \times F \times C_{NH3} \times V/(17 \times Q) \times 100\% \quad (1\text{-}4)$$

where C_{NH3} is the measured NH_3 concentrations, respectively; V is the total volume of electrolyte, t is the time for electrocatalysis and m is the catalyst loading. F is the Faraday constant (96,485 C mol^{-1}); and Q (C) is the total charge passed through the working electrode.

The determination of NO_2^- was based on the reported literatures.[1,3] In detail, 0.4 g $C_6H_8N_2O_2S$ and 0.02 g $C_{12}H_{14}N_2 \cdot 2HCl$ were dissolved in 1 mL H_3PO_4 and 5 mL deionized water to prepare the color reagent. Then 0.1 mL of the color reagent was mixed with the 5 mL diluted electrolyte for 20 min. The absorbance of mixed solution at a wavelength of 540 nm was measured by UV-vis spectrophotometry. The calibration curve was obtained using a series of standard KNO_2 solutions and the FE of NO_2^- was calculated using the following equation:

$$FE_{NO2^-} = (2 \times F \times C_{NO2^-} \times V)/(46 \times Q) \times 100\% \quad (1\text{-}5)$$

where F is the Faraday constant (96,485 C·mol^{-1}), where C is the measured concentration of NO_2^- and Q is the quantity charge (C).

The amounts of CO and H_2 were quantified using an in-line gas chromatograph (GC, GC-2014

Shimadzu).

The calculation of hydrogen content

The hydrogen content in H-PdZn bimetallene can be calculated according to Vegard's law.[4] A more descriptive description is given by the relationship between lattice parameters and the composition of palladium hydride, as shown in Fig. S4. The H content (x) is proportional to the guest atom (x=H/(Pd+Zn)), and the H content can be calculated from the lattice expansion (lattice parameter, a) caused by the introduction of H according to the Vegard's law ($a = a_0 + 0.19x$ (Å)), where a_0 is the lattice constant (3.868 Å) of PdZn bimetallene. The constant 0.19 is derived from the lattice parameters of Pd (PDF# 46-1043), $PdH_{0.43}$ (PDF# 87-0637) and $PdH_{0.706}$ (PDF# 18-0951) according to Vegard's law.

The determination of d-band center

The Pd d-band center was determined from valence band spectrum with the Shirley background subtraction according to a model presented in the literatures (d band center = $\int N(\varepsilon)\varepsilon d\varepsilon / \int N(\varepsilon)d\varepsilon$,[5,6] where $N(\varepsilon)$ is the XPS-intensity after background subtraction).

Theoretical calculations

We utilized the Vienna ab initio simulation package (VASP) to perform density functional theory (DFT) calculations, utilizing projector augmented wave (PAW) potentials and setting a plane-wave cutoff energy at 520 eV.[7-9] The exchange-correlation functional was employed by generalized gradient approximation (GGA) functional of Perdew, Burke, and Ernzerhof (PBE) with Grimme's semiempirical DFT-D3 dispersion correction to account for van der Waals (vdW) interactions.[10] Energy and force convergence criteria for structure optimization were set to 10^{-5} eV and 0.02 eV $Å^{-1}$, respectively. A bulk Pd model was constructed using the Fm-3m space group, followed by the

creation of a four-layer supercell for the Pd(111) model, with the vacuum layer of 16 Å. Subsequently, a certain amount of Zn atoms was randomly replaced with Pd atoms to build the PdZn(111) model. Then H atoms were embedded into the lattice of Pd to establish H-PdZn(111) model. The Gibbs free energy change (ΔG) for urea electrosynthesis was determined using the formula ($\Delta G = \Delta E + \Delta ZPE - T\Delta S$), where ΔE represented the difference of the adsorption energy, while ΔZPE and ΔS signify the changes of zero-point energy and entropy, respectively. The computational hydrogen electrode (CHE) model was used for the ΔG of the electrochemical reaction steps.[11] The VASPKIT code was employed for post-processing of the computational data,[12] while the VESTA package was used for visualization of the crystal structure.[13]

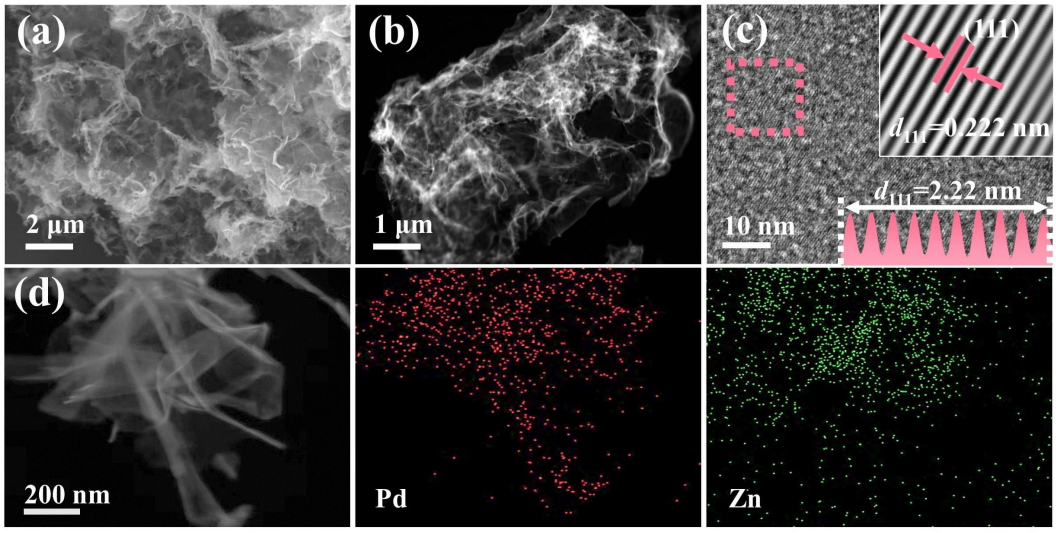

Fig. S1 (a) SEM and (b) HAADF-TEM images of PdZn bimetallene. (c) HRTEM image and the insets in (c) are the corresponding FFT pattern and the lattice distance. (d) HAADF-STEM image and the corresponding elemental mapping images of PdZn bimetallene.

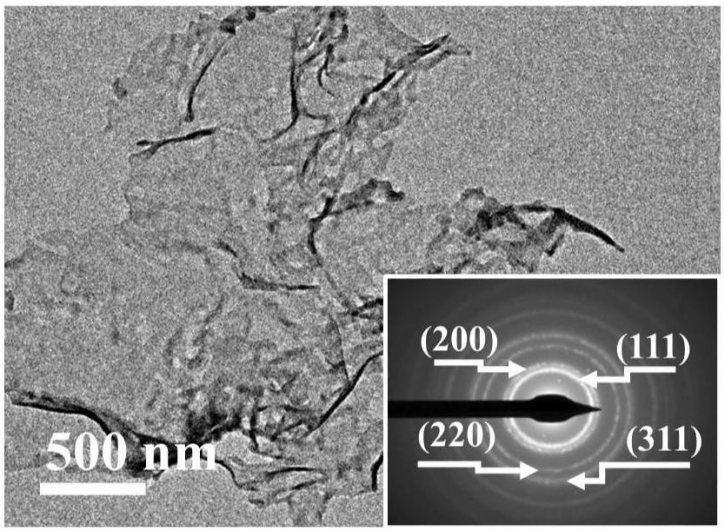

Fig. S2 TEM image of H-PdZn bimetallene and corresponding SAED pattern.

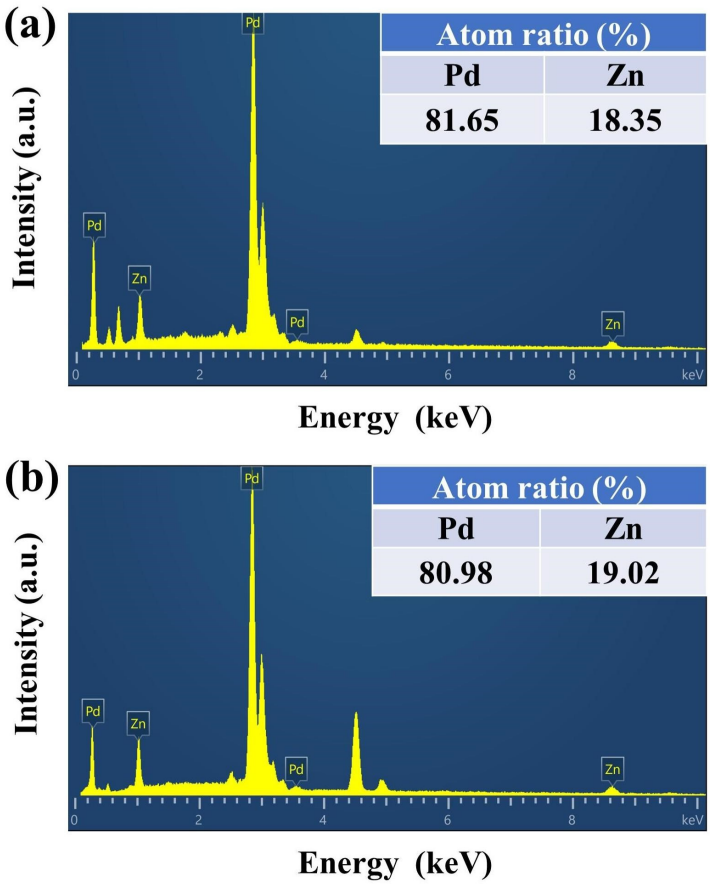

Fig. S3 The EDS spectra of samples and corresponding atom ratios of Pd and Zn.

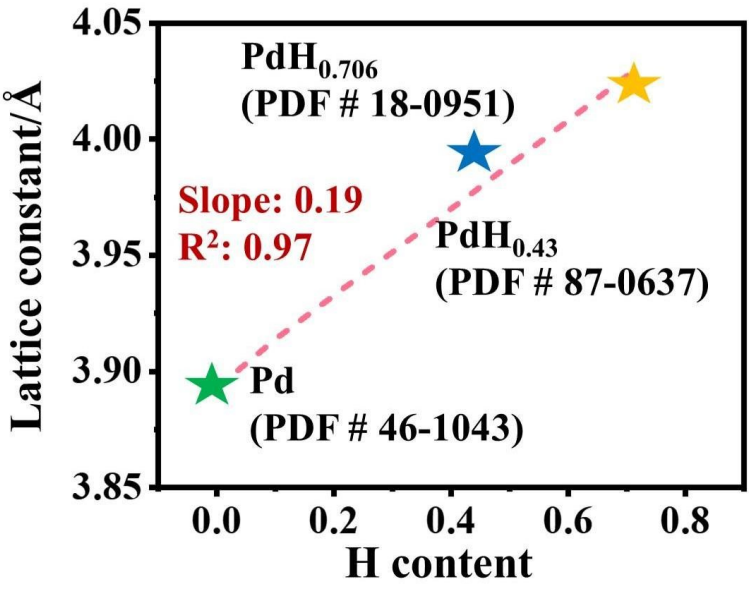

Fig. S4 The relationship between lattice constant and H content for PdH_x.

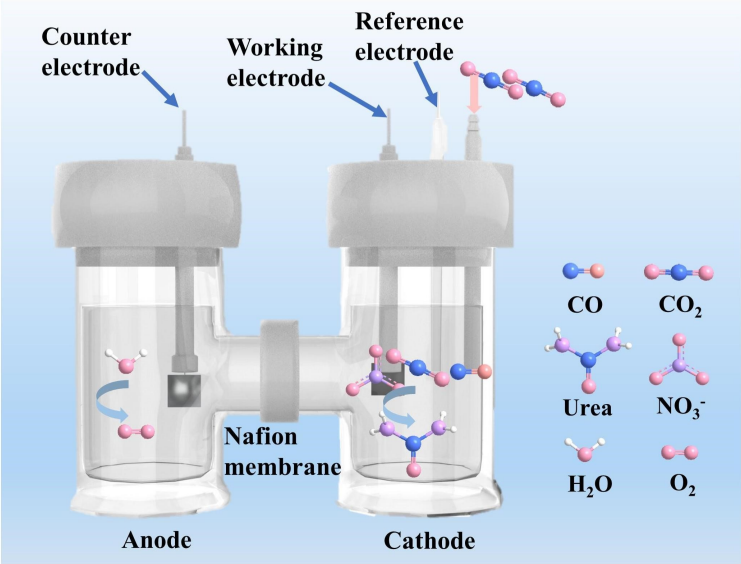

Fig. S5 Scheme of the urea electro-synthesis by coupling CO_2RR with NO_3RR on H-PdZn bimetallene.

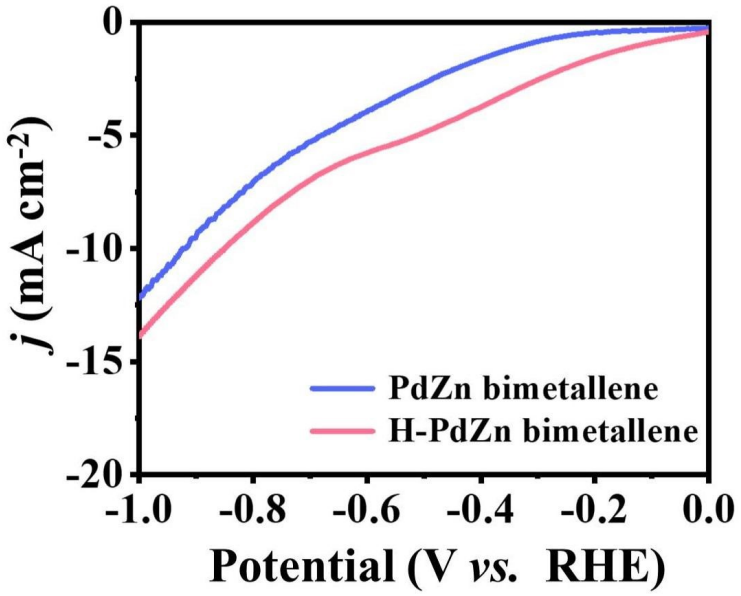

Fig. S6 LSV curves of H-PdZn bimetallene and PdZn bimetallene in 0.1 M KNO_3 electrolyte with CO_2 feeding.

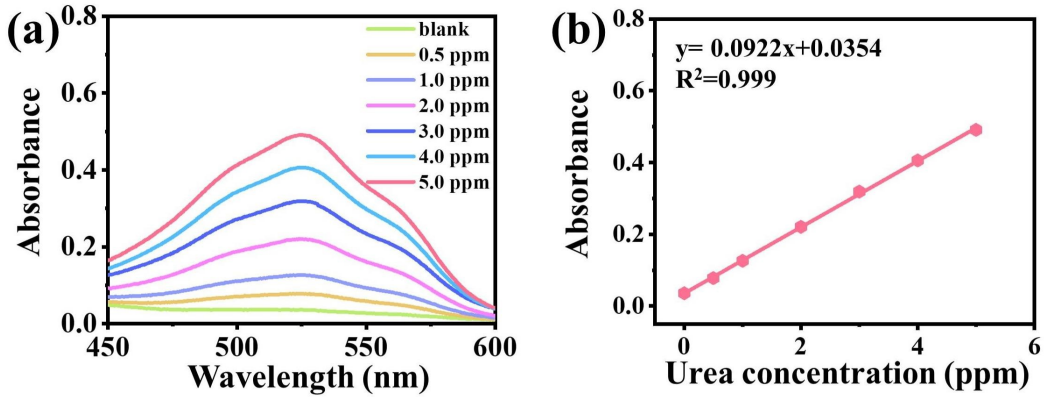

Fig. S7 (a) UV-vis absorption spectra of different concentrations of urea solutions (0, 0.5, 1.0, 2.0, 3.0, 4.0 and 5.0 ppm) after heating at 110 °C for 15 min. (b) Calibration curve used to estimate concentration of urea.

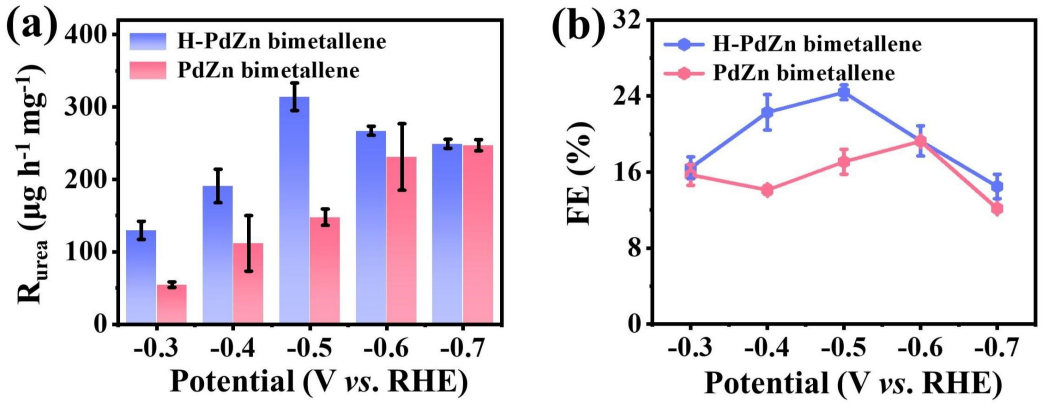

Fig. S8 (a) R_{urea} values of samples at different potentials in 0.1 M KNO_3 electrolyte with CO_2 feeding. (b) Faraday efficiencies of samples at -0.5 V.

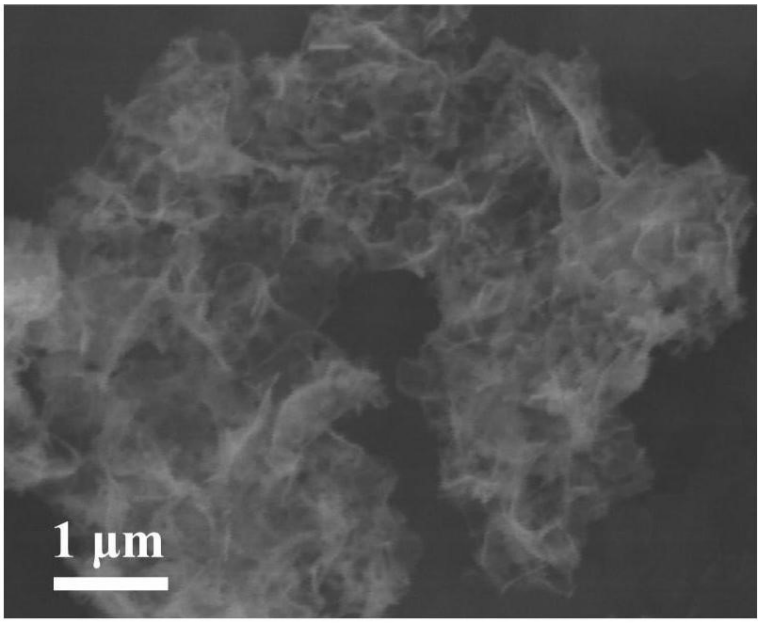

Fig. S9 (a) SEM images of H-PdZn bimetallene after testing.

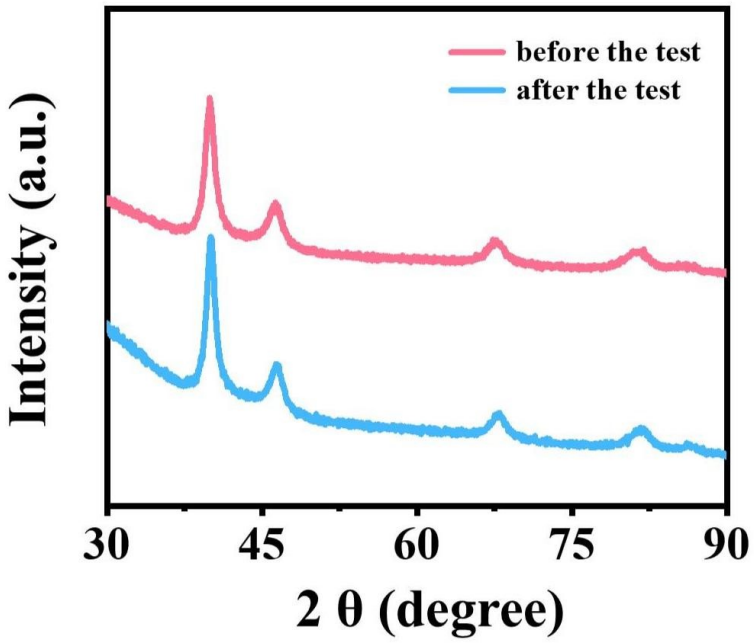

Fig. S10 (a) XRD images of H-PdZn bimetallene after and before the testing.

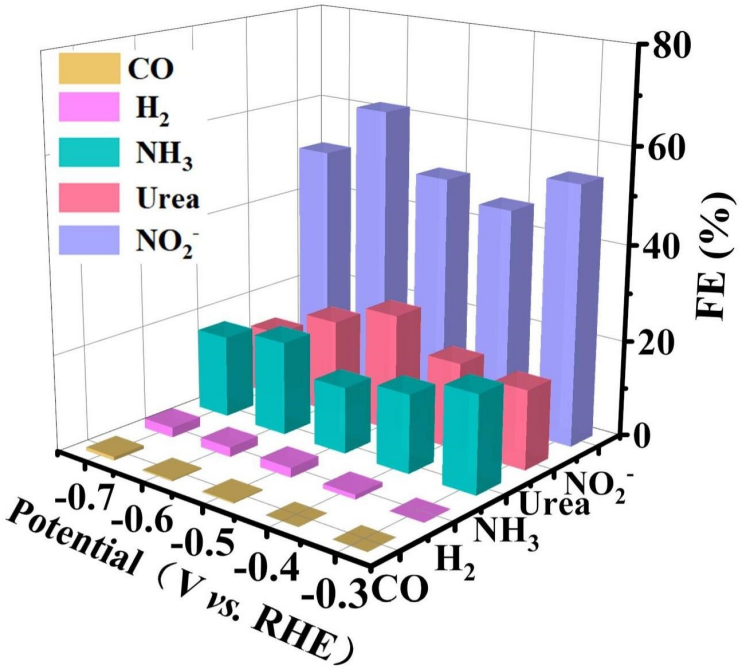

Fig. S11 FE values of different products on the H-PdZn bimetallene at various potentials.

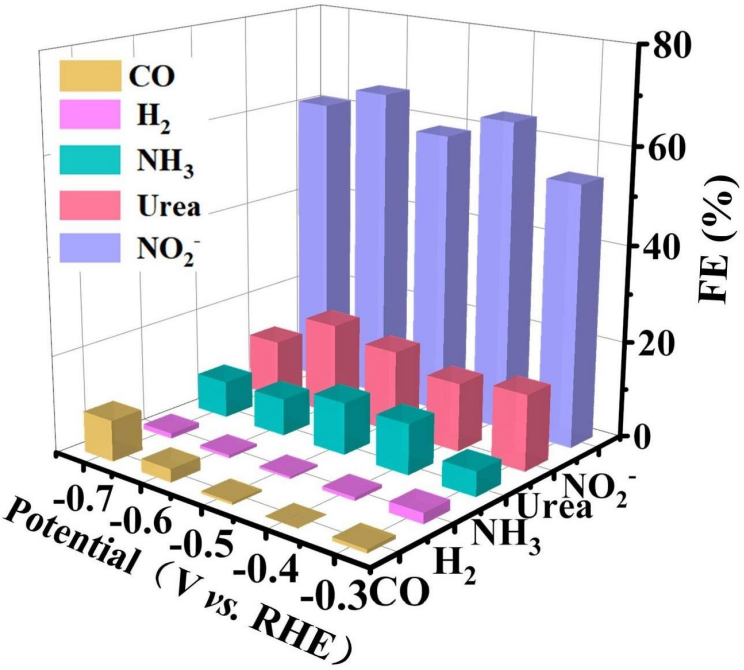

Fig. S12 FE values of different products on the PdZn bimetallene at various potentials.

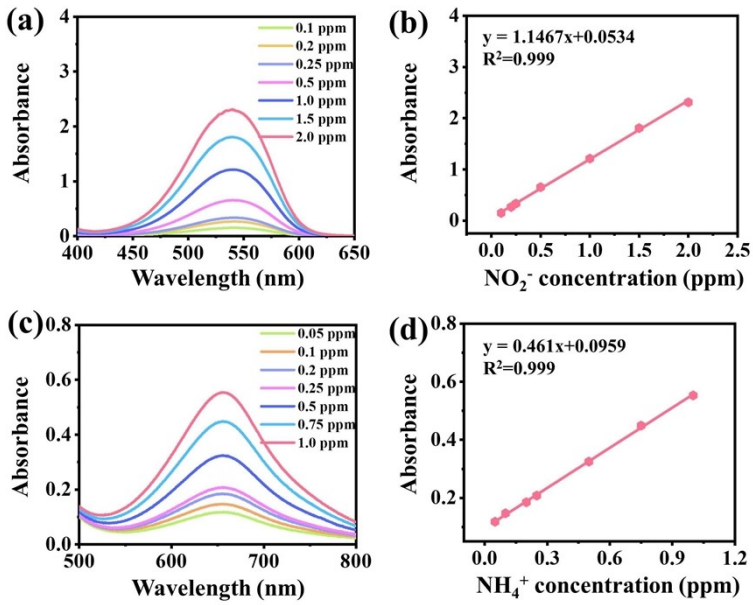

Fig. S13 (a) UV-vis absorption spectra of different concentrations of NO_2^- solutions and (b) corresponding calibration curve. (c) UV-vis absorption spectra of different concentrations of NH_4^+ solutions and (d) corresponding calibration curve.

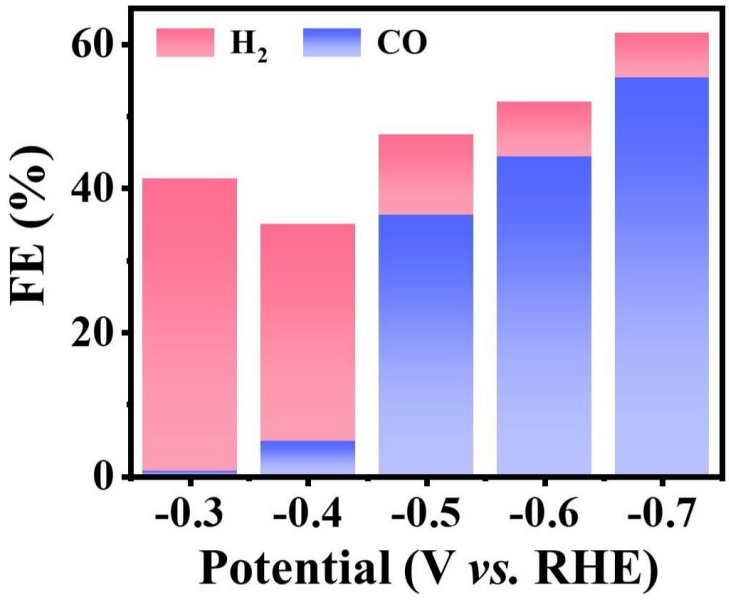

Fig. S14 FE values of H_2 and CO production after electrolysis in CO_2-saturated 0.1 M $KHCO_3$.

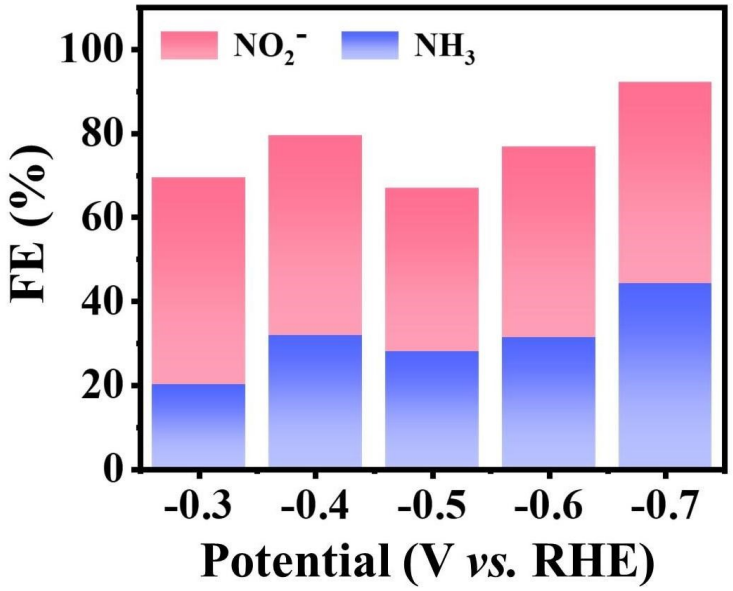

Fig. S15 FE values of the formation of NO_2^- and NH_3 after electrolysis in CO_2-saturated 0.1 M $KHCO_3$.

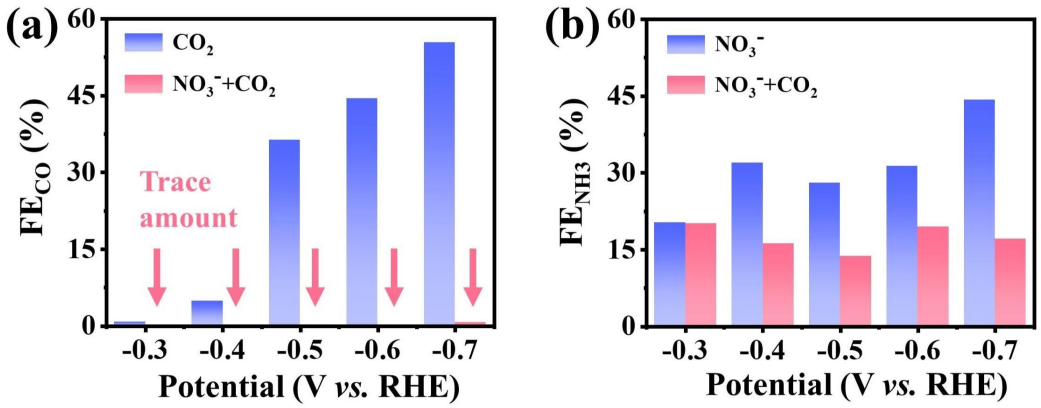

Fig. S16 (a) Faradaic efficiencies for CO production after electrolysis in 0.1 M $KHCO_3$ with CO_2 and 0.1 M KNO_3 with CO_2 on H-PdZn bimetallene. (b) Faradaic efficiencies for NH_3 synthesis after electrolysis in KNO_3 without CO_2 and with CO_2 over the H-PdZn bimetallene.

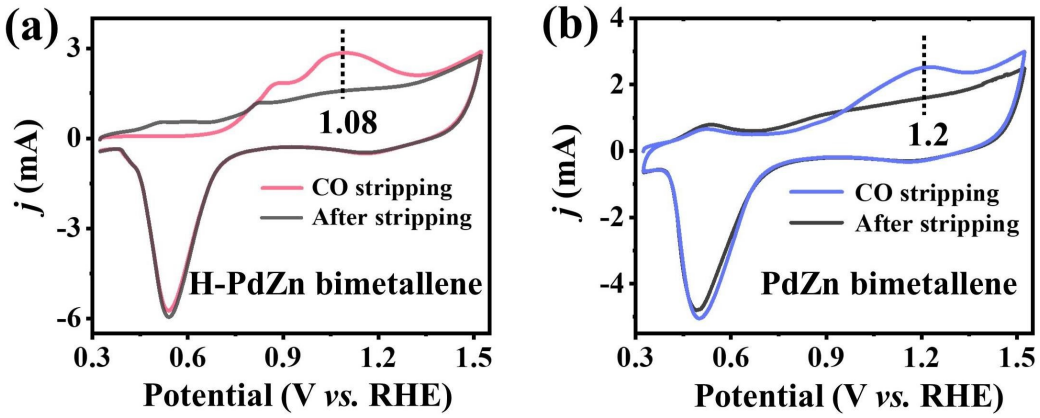

Fig. S17 CO stripping voltammetry curves of (a) H-PdZn bimetallene and (b) PdZn bimetallene in 1 M KOH with a scan rate of 50 mV s^{-1}.

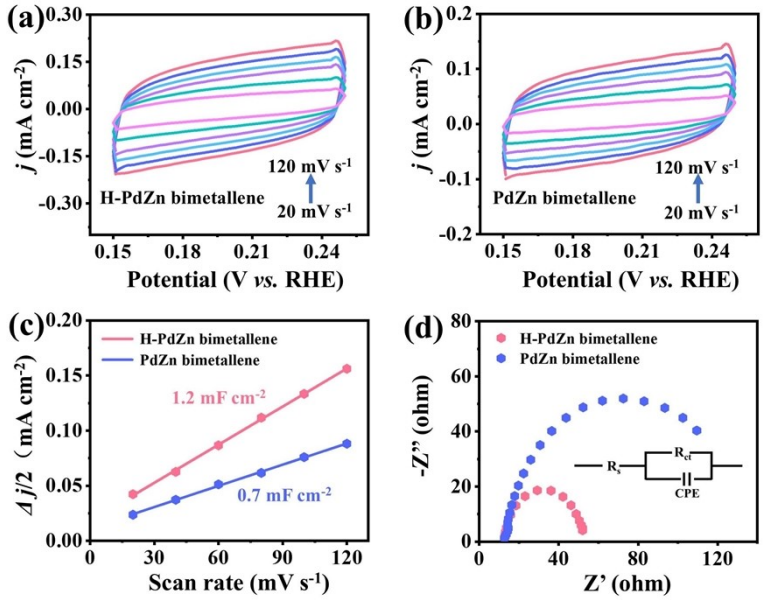

Fig. S18 Cyclic voltammogram curves for (a) H-PdZn bimetallene (b) PdZn bimetallene at various scan rates. (c) Plots of the current density versus the scan rate for H-PdZn bimetallene and PdZn bimetallene. (d) Nyquist plots of samples at -0.5 V in CO_2-saturated 0.1 M KNO_3.

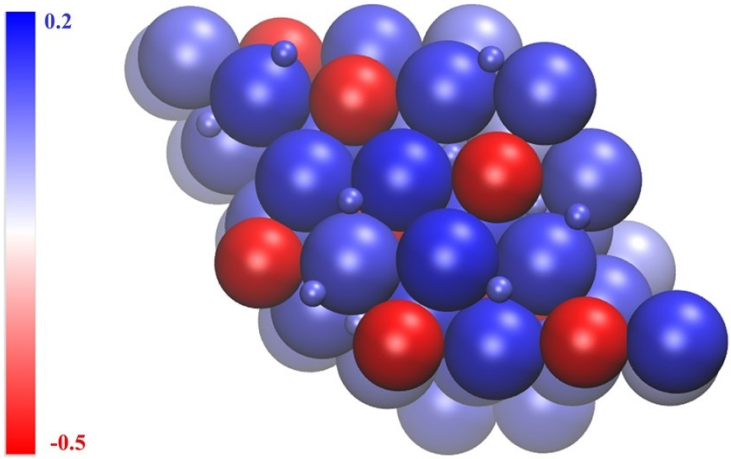

Fig. S19 Visualizing graph for Bader charge of H-PdZn bimetallene.

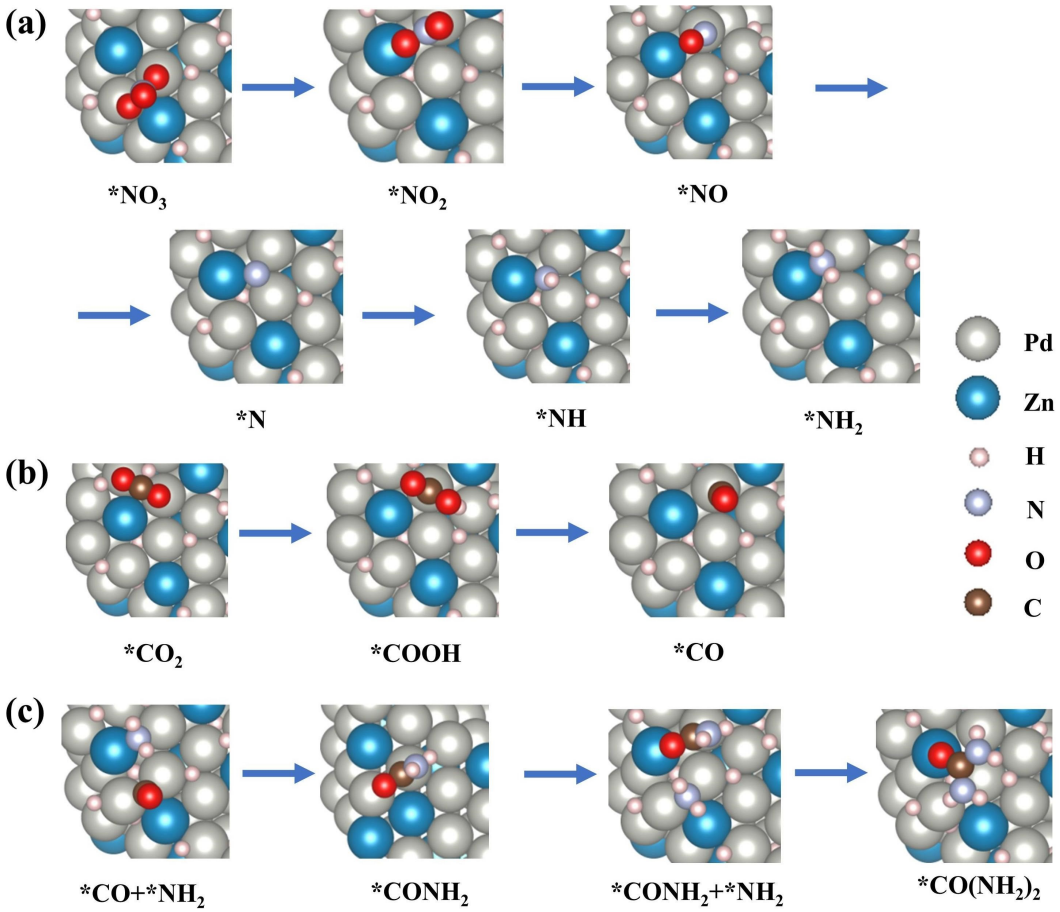

Fig. S20 Optimized structural models of H-PdZn bimetallene for electrocatalytic (a) nitrate reduction reaction, (b) carbon dioxide reduction reaction and (c) C-N coupling reaction.

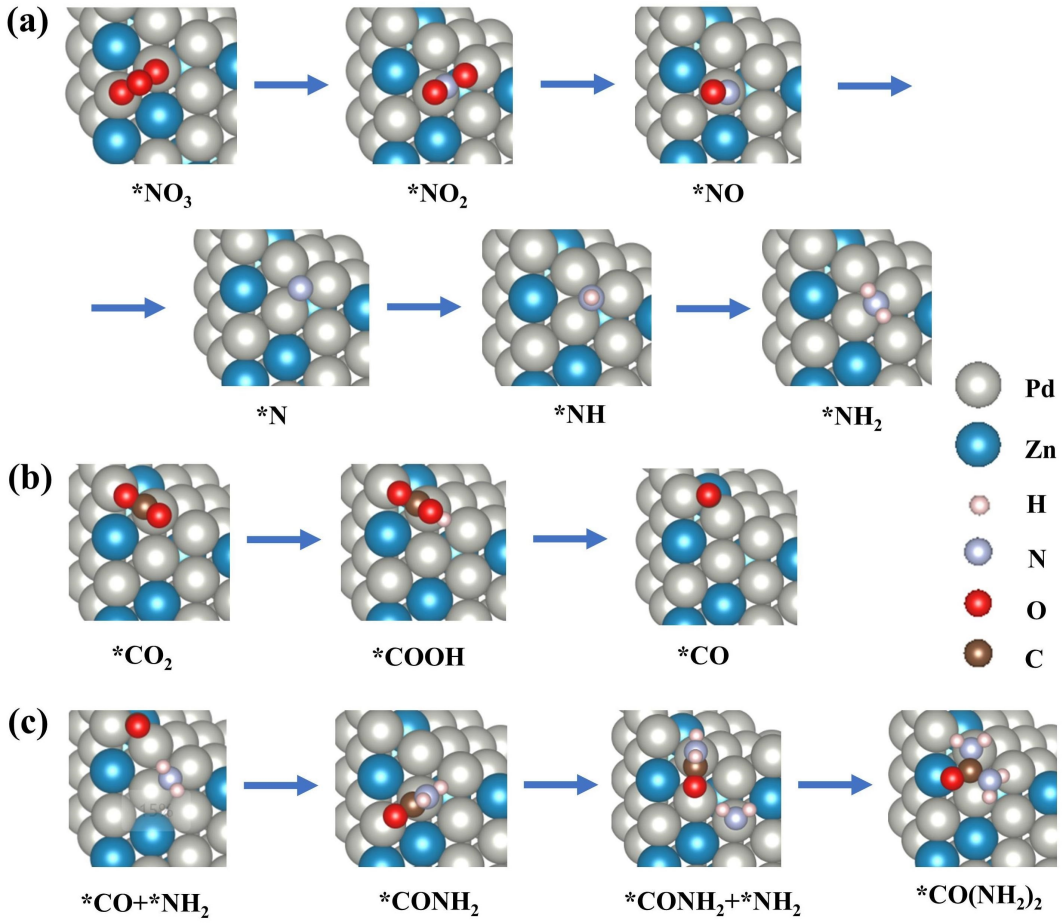

Fig. S21 Optimized structural models of PdZn bimetallene for electrocatalytic (a) nitrate reduction reaction, (b) carbon dioxide reduction reaction and (c) C-N coupling reaction.

Table S1. Electrocatalytic urea synthesis from N_2 and CO_2 co-reduction on heterogeneous catalytic systems in published works.

Catalyst	Electrolyte	FE_{urea}	R_{urea}	Potential	Reference
$PdCu/TiO_2$	0.1 M $KHCO_3$	8.92	3.36 mmol g^{-1} h^{-1}	-0.4	14
$Bi/BiVO_4$	0.1 M $KHCO_3$	12.55	5.91 mmol g^{-1} h^{-1}	-0.4	15
$BiFeO_3/BiVO_4$	0.1 M $KHCO_3$	17.18	4.94 mmol g^{-1} h^{-1}	-0.4	16
$Ni_3(BO_3)_2$-150	0.1 M $KHCO_3$	20.36	9.70 mmol h^{-1} g^{-1}	-0.5	17
Cu-Bi alloy	0.1 M $KHCO_3$	8.7	5.27 mol s^{-1} cm^2	-0.4	18
Rice-like InOOH	0.1 M $KHCO_3$	20.97	6.85 mmol h^{-1} g^{-1}	-0.4	19

Table S2. Electrocatalytic urea synthesis from nitrogen oxides and CO_2 co-reduction on heterogeneous catalytic systems in published works.

Catalyst	Reactants	FE_{urea} (%)	R_{urea}	Potential (V vs. RHE)	Reference
Te-Pd NCs	NO_2^- + CO_2	12.2	-	-1.1	20
Cu-TiO_2-Vo	NO_2^- + CO_2	43.1	20.8 μmol h^{-1}	-0.4	21
ZnO-Vo	NO_2^- + CO_2	23.26	16.56 μmol h^{-1}	-0.79	22
Zn nanobelts	NO + CO_2	11.26	15.13 mmol g^{-1} h^{-1}	-0.92	23
V_O-InOOH	NO_3^- + CO_2	51.0	592.5 μg h^{-1} mg^{-1}	-0.5	2
Cu@Zn	NO_3^- + CO_2	9.28	7.29 μmol cm^{-2} h^{-1}	-1.02	24
Vo-CeO_2-750	NO_3^- + CO_2	-	943.6 μg h^{-1} mg^{-1}	-1.6	25
B-FeNi-DASC	NO_3^- + CO_2	17.8	20.2 mmol h^{-1} g^{-1}	-1.5	26
AuPd	NO_3^- + CO_2	15.6	204.2 μg mg^{-1} h^{-1}	-0.5	27
H-PdZn bimetallene	**NO_3^- + CO_2**	**24.39**	**314.17 μg mg^{-1} h^{-1}**	**-0.5**	**This work**

References

1 Y. Zhao, Y. Ding, W. Li, C. Liu, Y. Li, Z. Zhao, Y. Shan, F. Li, L. Sun and F. Li, *Nat. Commun.*, 2023, **14**, 4491.

2 C. Lv, C. Lee, L. Zhong, H. Liu, J. Liu, L. Yang, C. Yan, W. Yu, H. H. Hng, Z. Qi, L. Song, S. Li, K. P. Loh, Q. Yan and G. Yu, *ACS Nano*, 2022, **16**, 8213-8222.

3 L. Lv, H. Tan, Y. Kong, B. Tang, Q. Ji, Y. Liu, C. Wang, Z. Zhuang, H. Wang, M. Ge, M. Fan, D. Wang and W. Yan, *Angew. Chem., Int. Ed.*, 2024, **63**, e202401943.

4 J. Fan, J. Wu, X. Cui, L. Gu, Q. Zhang, F. Meng, B.-H. Lei, D. J. Singh and W. Zheng, *J. Am. Chem. Soc.*, 2020, **142**, 3645-3651.

5 S. J. Hwang, S.-K. Kim, J.-G. Lee, S.-C. Lee, J. H. Jang, P. Kim, T.-H. Lim, Y.-E. Sung and S. J. Yoo, *J. Am. Chem. Soc.*, 2012, **134**, 19508-19511.

6 W. P. Zhou, A. Lewera, R. Larsen, R. I. Masel, P. S. Bagus and A. Wieckowski, *J. Phys. Chem. B*, 2006, **110**, 13393-13398.

7 G. Kresse and J. Furthmuller, *Comput. Mater. Sci*, 1996, **6**, 15-50.

8 G. Kresse and J. Hafner, *Phys. Rev. B*, 1993, **47**, 558-561.

9 P. E. Blöchl, *Phys. Rev. B*, 1994, **50**, 17953-17979.

10 J. P. Perdew, K. Burke and M. Ernzerhof, *Phys. Rev. Lett.*, 1996, **77**, 3865-3868.

11 J. K. Nørskov, J. Rossmeisl, A. Logadottir, L. Lindqvist, J. R. Kitchin, T. Bligaard and H. Jonsson, *J. Phys. Chem. B*, 2004, **108**, 17886-17892.

12 V. Wang, N. Xu, J.-C. Liu, G. Tang and W.-T. Geng, *Comput. Phys. Commun.*, 2021, **267**, 108033.

13 K. Momma and F. Izumi, *J. Appl. Crystallogr.*, 2011, **44**, 1272-1276.

14 C. Chen, X. Zhu, X. Wen, Y. Zhou, L. Zhou, H. Li, L. Tao, Q. Li, S. Du, T. Liu, D. Yan, C. Xie, Y. Zou, Y. Wang, R. Chen, J. Huo, Y. Li, J. Cheng, H. Su, X. Zhao, W. Cheng, Q. Liu, H. Lin, J. Luo, J. Chen, M. Dong, K. Cheng, C. Li and S. Wang, *Nat. Chem*., 2020, **12**, 717-724.

15 M. Yuan, J. Chen, Y. Bai, Z. Liu, J. Zhang, T. Zhao, Q. Wang, S. Li, H. He and G. Zhang, *Angew. Chem., Int. Ed.*, 2021, **60**, 10910-10918.

16 M. Yuan, J. Chen, Y. Bai, Z. Liu, J. Zhang, T. Zhao, Q. Shi, S. Li, X. Wang and G. Zhang, *Chem. Sci.*, 2021, **12**, 6048-6058.

17 M. Yuan, J. Chen, Y. Xu, R. Liu, T. Zhao, J. Zhang, Z. Ren, Z. Liu, C. Streb, H. He, C. Yang, S. Zhang and G. Zhang, *Energy Environ. Sci.,* 2021, **14**, 6605-6615.

18 W. Wu, Y. Yang, Y. Wang, T. Lu, Q. Dong, J. Zhao, J. Niu, Q. Liu, Z. Hao and S. Song, *Chem Catal.*, 2022, **2**, 3225-3238.

19 M. Yuan, H. Zhang, Y. Xu, R. Liu, R. Wang, T. Zhao, J. Zhang, Z. Liu, H. He, C. Yang, S. Zhang and G. Zhang, *Chem Catal.*, 2022, **2**, 309-320.

20 Y. Feng, H. Yang, Y. Zhang, X. Huang, L. Li, T. Cheng and Q. Shao, *Nano Lett.*, 2020, **20**, 8282-8289.

21 N. Cao, Y. Quan, A. Guan, C. Yang, Y. Ji, L. Zhang and G. Zheng, *J. Colloid Interface Sci.*, 2020, **577**, 109-114.

22 N. Meng, Y. Huang, Y. Liu, Y. Yu and B. Zhang, *Cell Rep. Phys. Sci.,* 2021, **2**, 100378.

23 Y. Huang, R. Yang, C. Wang, N. Meng, Y. Shi, Y. Yu and B. Zhang, *ACS Energy Lett.*, 2022, **7**, 284-291.

24 N. Meng, X. Ma, C. Wang, Y. Wang, R. Yang, J. Shao, Y. Huang, Y. Xu, B. Zhang and Y. Yu, *ACS Nano*, 2022, **16**, 9095-9104.

25 X. Wei, X. Wen, Y. Liu, C. Chen, C. Xie, D. Wang, M. Qiu, N. He, P. Zhou, W. Chen, J. Cheng, H. Lin, J. Jia, X.-Z. Fu and S. Wang, *J. Am. Chem. Soc.*, 2022, **144**, 11530-11535.

26 X. Zhang, X. Zhu, S. Bo, C. Chen, M. Qiu, X. Wei, N. He, C. Xie, W. Chen, J. Zheng, P. Chen, S. P. Jiang, Y. Li, Q. Liu and S. Wang, *Nat. Commun.*, 2022, **13**, 5337.

27 H. Wang, Y. Jiang, S. Li, F. Gou, X. Liu, Y. Jiang, W. Luo, W. Shen, R. He and M. Li, *Appl. Catal., B*, 2022, **318**, 121819.